Crystal structure of tofacitinib dihydrogen citrate (Xeljanz®), ($C_{16}H_{21}N_6O$)($H_2C_6H_5O_7$)

James A. Kaduk,[1,2,a] Amy M. Gindhart,[3] and Thomas N. Blanton[3]
[1]North Central College, 131 S. Loomis St., Naperville, Illinois 60540, USA
[2]Illinois Institute of Technology, 3101 S. Dearborn St., Chicago, Illinois 60616, USA
[3]ICDD, 12 Campus Blvd., Newtown Square, Pennsylvania 19073-3273, USA

(Received 18 November 2020; accepted 10 January 2021)

The crystal structure of tofacitinib dihydrogen citrate (tofacitinib citrate) has been solved and refined using synchrotron X-ray powder diffraction data, and optimized using density functional techniques. Tofacitinib dihydrogen citrate crystallizes in space group $P2_12_12_1$ (#19) with $a = 5.91113(1)$, $b = 12.93131(3)$, $c = 30.43499(7)$ Å, $V = 2326.411(6)$ Å^3, and $Z = 4$. The crystal structure consists of corrugated layers perpendicular to the *c*-axis. Within the layers, cation···anion and anion···anion hydrogen bonds link the fragments into a two-dimensional network parallel to the *ab*-plane. Between the layers, there are only van der Waals contacts. A terminal carboxylic acid group in the citrate anion forms a strong charge-assisted hydrogen bond to the ionized central carboxylate group. The other carboxylic acid acts as a donor to the carbonyl group of the cation. The citrate hydroxy group forms an intramolecular charge-assisted hydrogen bond to the ionized central carboxylate. Two protonated nitrogen atoms in the cation act as donors to the ionized central carboxylate of the anion. These hydrogen bonds form a ring with the graph set symbol *R2,2(8)*. The powder pattern has been submitted to ICDD® for inclusion in the Powder Diffraction File™ (PDF®).
[doi:10.1017/S0885715621000105]

Key words: tofacitinib citrate, Xeljanz®, Rietveld refinement, density functional theory

I. INTRODUCTION

Tofacitinib citrate, marketed under the brand names Xeljanz® and others, is used to treat rheumatoid and psoriatic arthritis. Tofacitinib works by blocking the body's production of enzymes called Janus kinases (JAKs), specifically JAK1 and JAK3. Tofacitinib citrate is also prescribed to treat ulcerative colitis. The IUPAC name (CAS Registry number 540737-29-9) is 3-[(3*R*,4*R*)-4-methyl-3-[methyl(7H-pyrrolo [2,3-d]pyrimidin-4-yl)amino]piperidin-1-yl]-3-oxopropanenitrile 2-hydroxypropane-1,2,3-tricarboxylic acid. The molecular structure of tofacitinib citrate is illustrated in Figure 1. The literature indicates that it is a 1:1 salt, so is better named tofacitinib dihydrogen citrate.

Tofacitinib citrate was claimed in International Patent Applications WO 01/42246 A2 (Blumenkopf *et al.*, 2001) and WO 02/096909 A1 (Wilcox *et al.*, 2002), but no powder diffraction data were provided. A powder pattern is included in European Patent EP 1451192 B1 (Flanagan and Li, 2002). A similar powder pattern is reported in International Patent Application WO 2015/051738 A1 (Lei *et al.*, 2015). Many other crystalline and amorphous salts of tofacitinib are claimed in the patent literature.

This work was carried out as part of a project (Kaduk *et al.*, 2014) to determine the crystal structures of large-volume commercial pharmaceuticals and include high-quality powder diffraction data for these pharmaceuticals in the Powder Diffraction File (Gates-Rector and Blanton, 2019).

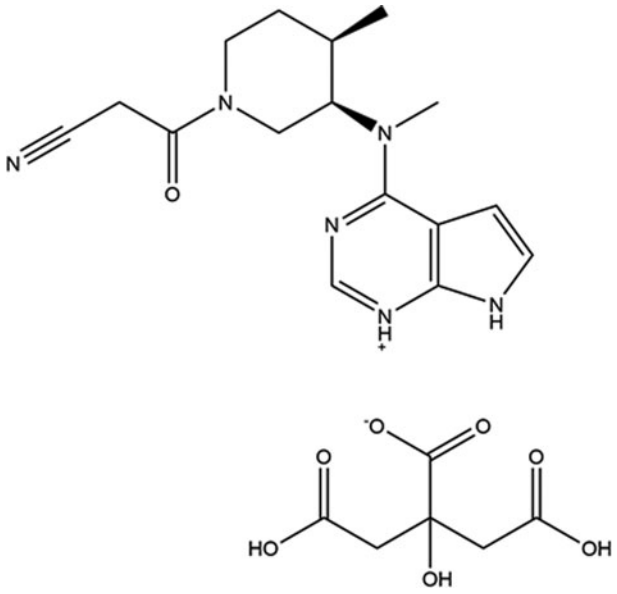

Figure 1. The molecular structure of tofacitinib dihydrogen citrate.

II. EXPERIMENTAL

The sample was a commercial reagent, purchased from Sigma (Lot #0000068911), and was used as-received. The

[a]Author to whom correspondence should be addressed. Electronic mail: kaduk@polycrystallography.com

white powder was packed into a 1.5-mm diameter Kapton capillary and rotated during the measurement at ~50 Hz. The powder pattern was measured at 295 K at beamline 11-BM (Lee *et al.*, 2008; Wang *et al.*, 2008) of the Advanced Photon Source at Argonne National Laboratory using a wavelength of 0.457899 Å from 0.5° to 50° 2θ with a step size of 0.001° and a counting time of 0.1 s step^{-1}.

The pattern was indexed on a primitive orthorhombic unit cell with $a = 5.91175$, $b = 12.93239$, $c = 30.43566$ Å, $V = 2326.9$ Å^3, and $Z = 4$ using N-TREOR (Altomare *et al.*, 2013). The suggested space group was $P2_12_12_1$ (#19), which was confirmed by successful solution and refinement of the structure. A reduced cell search in the Cambridge Structural Database (Groom *et al.*, 2016) yielded 23 hits, but no structures for tofacitinib derivatives.

A neutral tofacitinib molecule was built using Spartan '18 (Wavefunction, 2020), saved as a .mol2 file, and the chirality was checked to ensure that it was correct. It was converted into a Fenske-Hall *Z*-matrix using OpenBabel (O'Boyle *et al.*, 2011). The structure was solved by Monte Carlo simulated annealing (parallel tempering) techniques as implemented in FOX (Favre-Nicolin and Černý, 2002), using a tofacitinib and a citrate (without the acidic and hydroxyl hydrogen atoms) as fragments. One of the 34 runs yielded a cost factor much lower than the others, and was used to begin refinement.

Once the structure was solved, the task of locating the "interesting" hydrogen atoms remained. The relative orientation of the cation and the anion (Figure 2) made the process easier. As noted in Rammohan and Kaduk (2018), the central carboxylic acid of citric acid almost always ionizes first. The negatively charged C49–O58–O59 carboxylate group meant that N35 was protonated in preference to other potential N atoms in the tofacitinib molecule. Thus, the terminal carboxyl groups of the citrate were protonated. Examining the O···O distances revealed that O56···O59 (negative carboxylate) = 2.667 Å, and O55···O21 (carbonyl) = 2.658 Å. O54 and O57 were not involved in any short O···O distances, so the acid protons were located on O56 and O55. Similar analysis of the O···O distances around the hydroxyl group O60 indicated that it formed an intramolecular hydrogen bond to the negatively charged O58. Approximate H positions were placed 0.85 Å from the bonded O on these O···O vectors, and later optimized by the density functional theory (DFT) calculation.

Rietveld refinement was carried out using GSAS-II (Toby and Von Dreele, 2013). Only the 1.5–27.0° portion of the pattern was included in the refinement ($d_{min} = 0.981$ Å). All non-H bond distances and angles were subjected to restraints, based on a Mercury/Mogul Geometry Check (Bruno *et al.*, 2004; Sykes *et al.*, 2011) of the model. The Mogul average and standard deviation for each quantity were used as the restraint parameters. The restraints contributed 6.6% to the final χ^2. The hydrogen atoms were included in calculated positions, which were recalculated during the refinement using Materials Studio (Dassault, 2020). The U_{iso} of the heavy atoms were grouped by chemical similarity. The U_{iso} of the hydrogen atoms were constrained to be 1.3× that of the heavy atoms to which they are attached. The background was modeled using a 6-term shifted Chebyshev polynomial, along with a peak at 5.85° to model the scattering from the Kapton capillary and any amorphous component of the sample. The peak profiles were described using the generalized

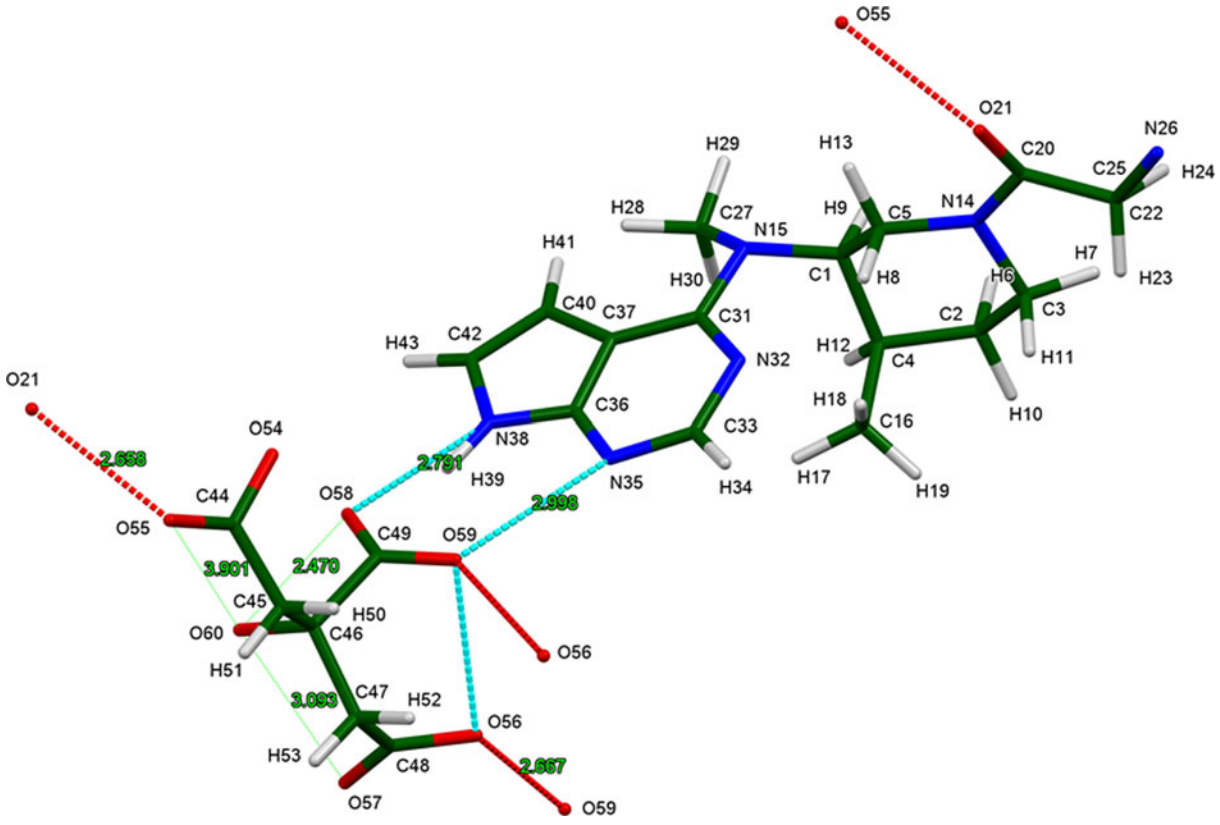

Figure 2. The close contacts (indicated by cyan and red dashed lines) between the tofacitinib cation and the citrate anion, contacts which permitted deduction of the "additional" protons in the cation and the anion.

https://doi.org/10.1017/S0885715621000105 Published online by Cambridge University Press

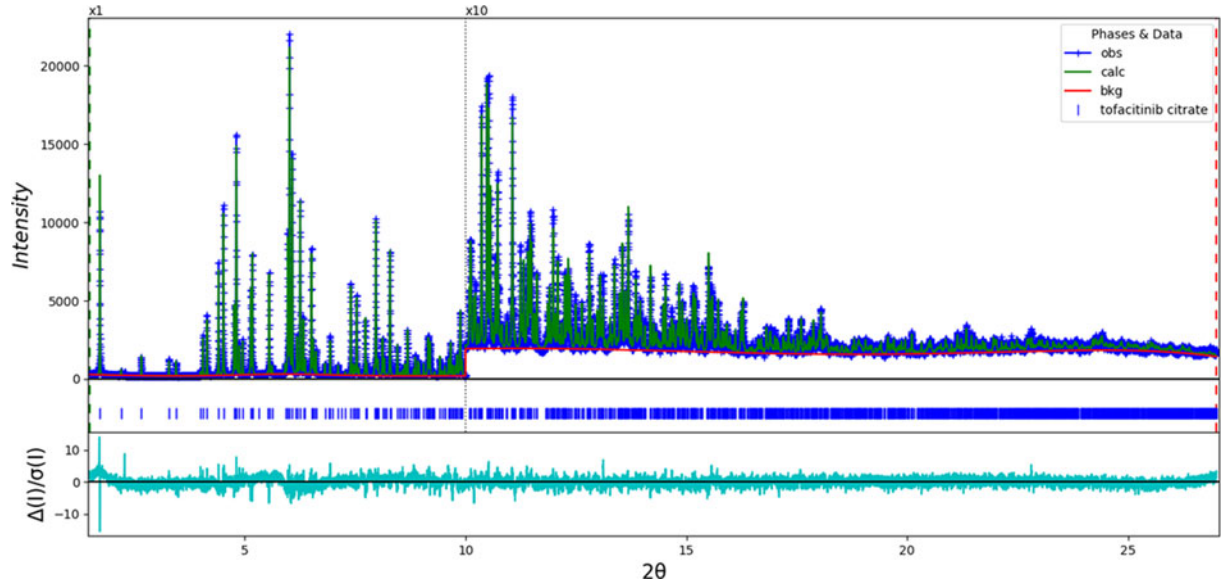

Figure 3. The Rietveld plot for the refinement of tofacitinib dihydrogen citrate. The blue crosses represent the observed data points, and the green line is the calculated pattern. The cyan curve is the normalized error plot. The vertical scale is multiplied by a factor of 10 for $2\theta > 10.0°$.

microstrain model, and a secnd-order spherical harmonic preferred orientation model was included.

The final refinement of 136 variables using 25 541 observations and 89 restraints yielded the residuals $R_{wp} = 0.0701$ and GOF = 1.39. The largest peak (0.72 Å from O21) and hole (0.70 Å from O57) in the difference Fourier map were 0.29 and −0.28(7) eÅ^{-3}, respectively. The largest errors in the fit (Figure 3) are in the shape of the lowest-angle peak. A weak unindexed peak at 2.29° indicates that an unidentified trace impurity is present, consistent with the stated purity of >98% in the Sigma catalog.

A density functional geometry optimization (fixed experimental unit cell) was carried using CRYSTAL14 (Dovesi *et al.*, 2014). The basis sets for the H, C, N, and O atoms were those of Gatti *et al.* (1994). The calculation was run on eight 2.1 GHz Xeon cores (each with 6 GB RAM) of a 304-core Dell Linux cluster at IIT, using 8 k-points and the B3LYP functional, and took ∼96 h.

III. RESULTS AND DISCUSSION

The synchrotron powder pattern from this study of tofacitinib dihydrogen citrate matches that reported by Flanagan and Li (2002) well enough to conclude that they represent the same material (Figure 4). The refined atom coordinates of tofacitinib dihydrogen citrate and the coordinates from the

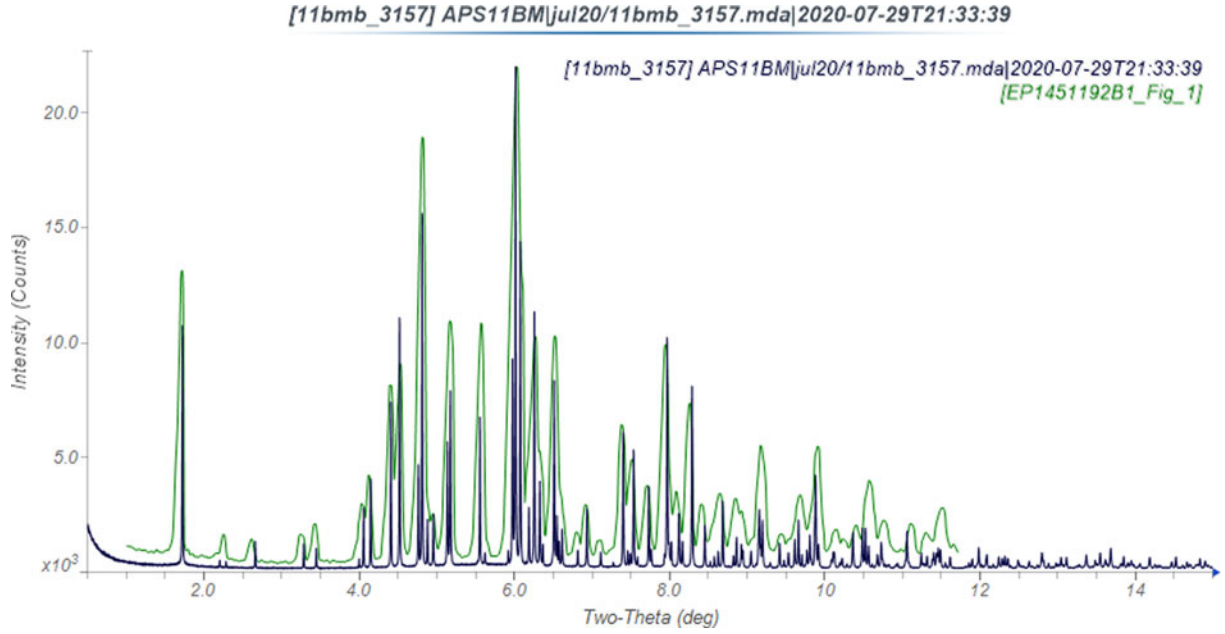

Figure 4. Comparison of the synchrotron pattern (black) of tofacitinib citrate to the experimental pattern (green) reported by Flanagan and Li (2002). The published pattern was digitized using UN-SCAN-IT (Silk Scientific, 2013) and scaled to the synchrotron wavelength of 0.457899 Å using MDI JADE Pro (MDI, 2020).

https://doi.org/10.1017/S0885715621000105 Published online by Cambridge University Press

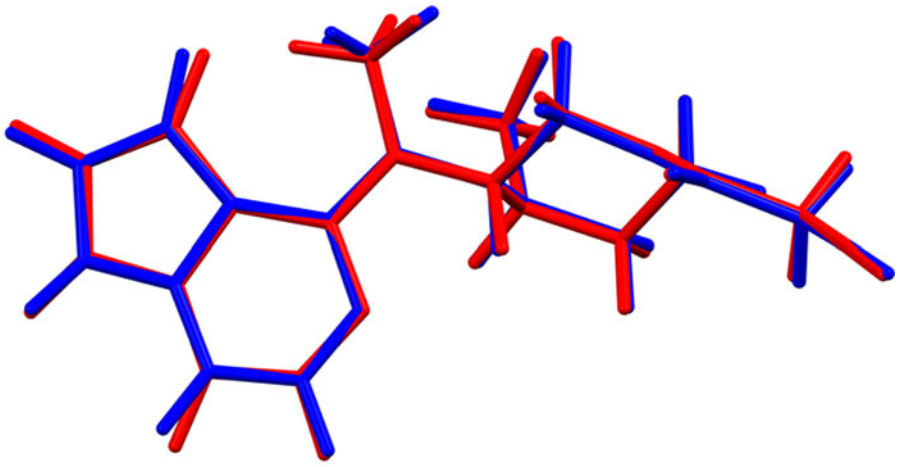

Figure 5. Comparison of the Rietveld-refined (red) and DFT (blue) structures of the tofacitinib cation in tofacitinib dihydrogen citrate.

DFT optimization are reported in the CIFs deposited with ICDD.

The root-mean-square (rms) Cartesian displacement of the non-hydrogen atoms in the Rietveld-refined and DFT-optimized cation structures of the cation is 0.071 Å (Figure 5), and the rms displacement for the citrate anion is 0.052 Å (Figure 6), and is well within the normal range for correct structures (van de Streek and Neumann, 2014). This discussion concentrates on the DFT-optimized structure. The asymmetric unit (with atom numbering) is illustrated in Figure 7, and the crystal structure is presented in Figure 8.

The crystal structure (Figure 8) consists of corrugated layers perpendicular to the *c*-axis. Within the layers, cation···anion and anion···anion hydrogen bonds link the fragments into a two-dimensional network parallel to the *ab*-plane. Between the layers, there are only van der Waals contacts.

Almost all of the bond distances, angles, and torsion angles fall within the normal ranges indicated by a Mercury/Mogul Geometry check (Macrae *et al.*, 2020). Only the C33–N32–C31 angle of 121.4 (average = 112.1(25)°, *Z*-score = 3.6) is flagged as unusual. This angle in the fused ring system lies in a minor population of the distribution.

Quantum chemical geometry optimization of the tofacitinib cation (DFT/B3LYP/6-31G*/water) using Spartan '18 (Wavefunction, 2020) indicated that the observed solid-state conformation is 4.1 kcal mol^{-1} higher in energy than the local minimum (Figure 9); the rms Cartesian displacement is 0.354 Å. The global minimum-energy conformation (MMFF, molecular mechanics force field) is lower in energy by 7.6 kcal mol^{-1} (Figure 10). The rms Cartesian displacement is 1.794 Å, indicating that intermolecular interactions are important in determining the observed solid-state conformation. The citrate anion is in the *trans,trans* conformation (about the C45–C46 and C46–C47 bonds), one of the two low-energy conformations of a citrate (Rammohan and Kaduk, 2018). The O58–C49–C46–O60 torsion angle is 3.4 degrees indicating that the central portion of the citrate is in the normal planar conformation.

Analysis of the contributions to the total lattice energy using the Forcite module of Materials Studio (Dassault, 2020) suggests that angle deformation terms are the dominant contributions to the intramolecular deformation energy, as expected for a molecule which contains a fused ring system. The intermolecular energy is dominated by electrostatic attractions, which in this force-field-based analysis include

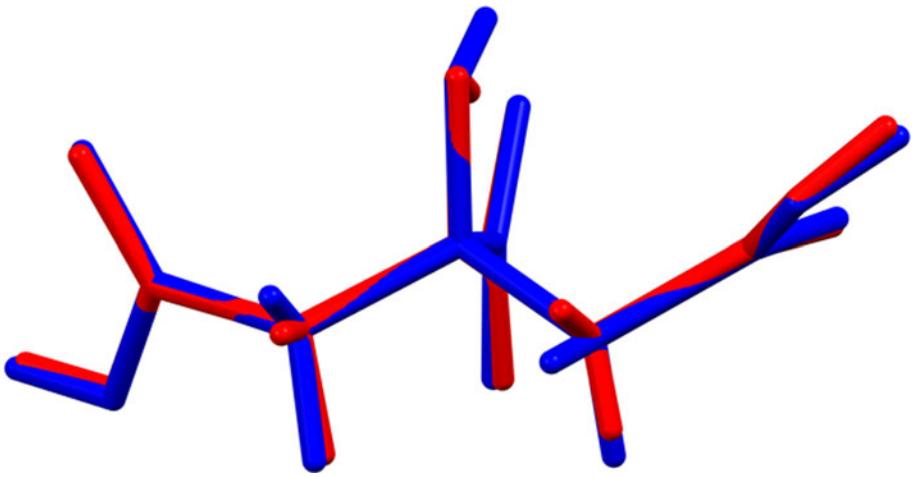

Figure 6. Comparison of the Rietveld-refined (red) and DFT (blue) structures of the dihydrogen citrate anion in tofacitinib dihydrogen citrate.

https://doi.org/10.1017/S0885715621000105 Published online by Cambridge University Press

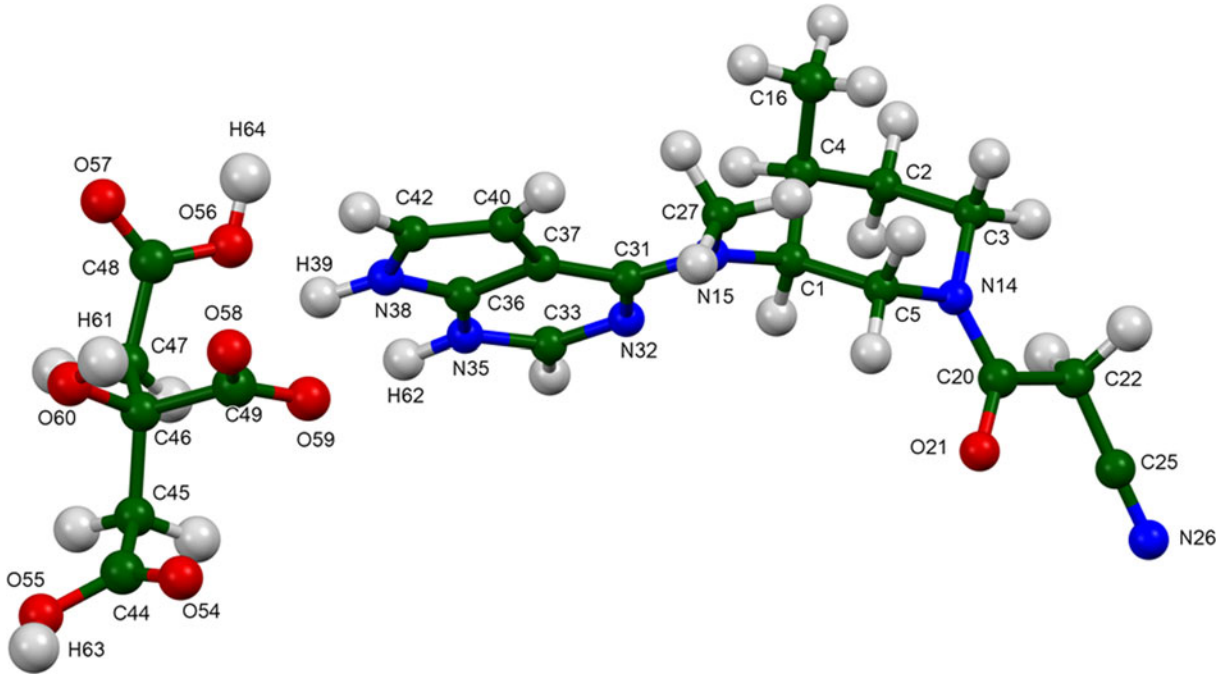

Figure 7. The asymmetric unit of tofacitinib dihydrogen citrate, with the atom numbering. The atoms are represented by 50% probability spheroids.

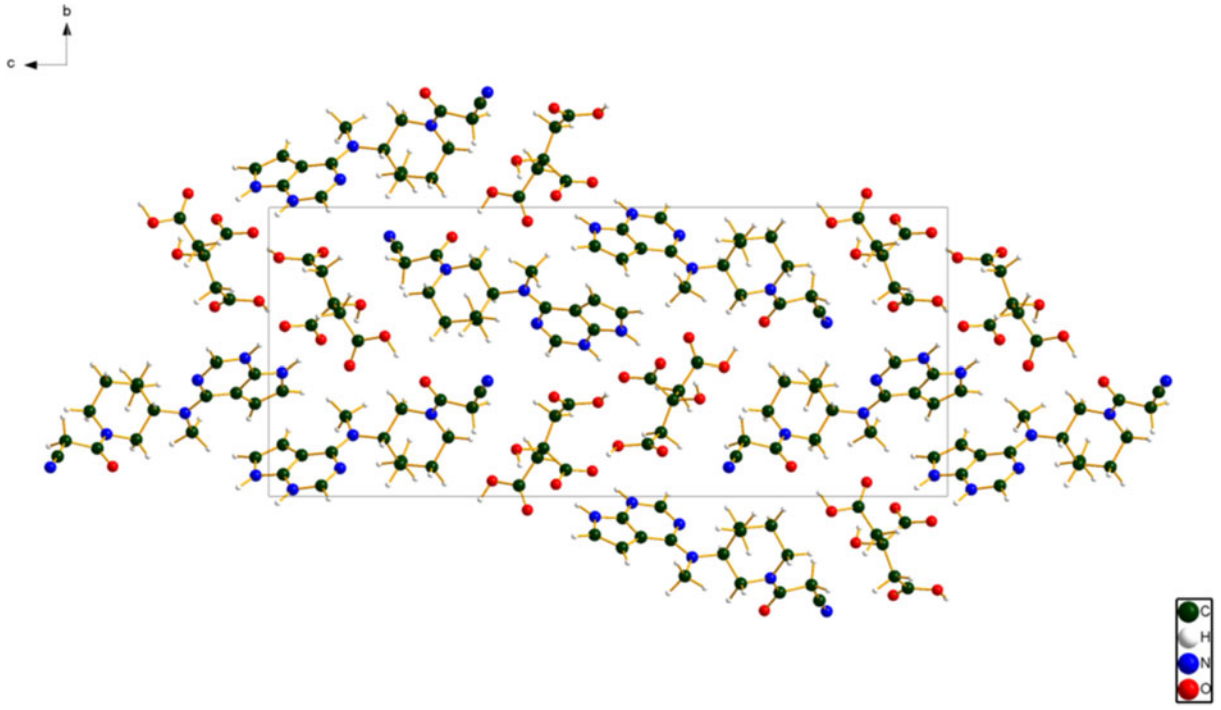

Figure 8. The crystal structure of tofacitinib dihydrogen citrate, viewed down the *a*-axis.

hydrogen bonds. The hydrogen bonds are better analyzed using the results of the DFT calculation.

As expected, hydrogen bonds are important in the crystal structure (Table I). The carboxylic acid O56–H64 forms a strong charge-assisted hydrogen bond to the ionized carboxylate O59. The other carboxylic acid O55–H63 acts as a donor to the carbonyl group O21. The citrate hydroxy group O60–H61 forms an intramolecular charge-assisted hydrogen bond to the ionized carboxylate O58. The two protonated nitrogen atoms N35–H62 and N38–H39 act as donors to the ionized carboxylate O59 and O58. These hydrogen bonds form a ring with the graph set symbol *R2,2(8)* (Etter, 1990; Bernstein *et al.*, 1995; Shields *et al.*, 2000). The energies of the O–H···O hydrogen bonds were calculated using the correlation of Rammohan and Kaduk (2018), and the energies of the N–H···O hydrogen bonds according to the correlation of

https://doi.org/10.1017/S0885715621000105 Published online by Cambridge University Press

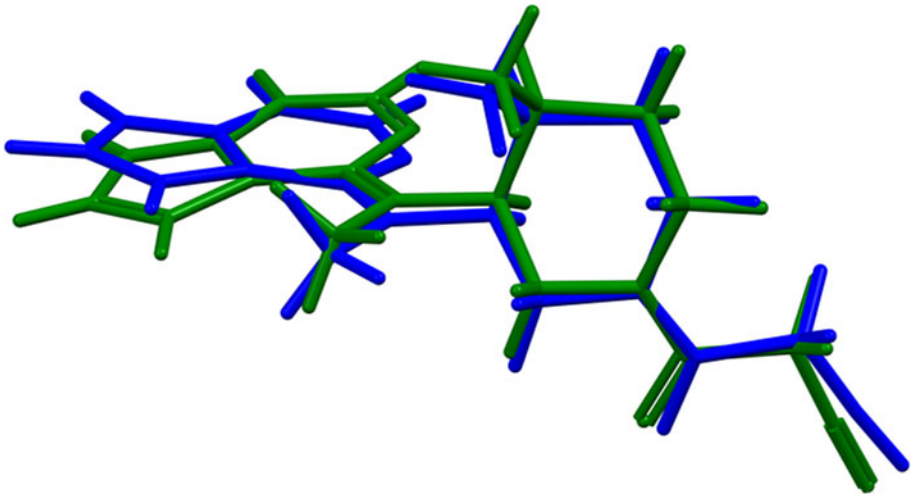

Figure 9. Comparison of the DFT-optimized solid-state conformation of the tofacitinib cation (blue) to the local minimum conformation (green). The rms cartesian displacement is 0.354 Å.

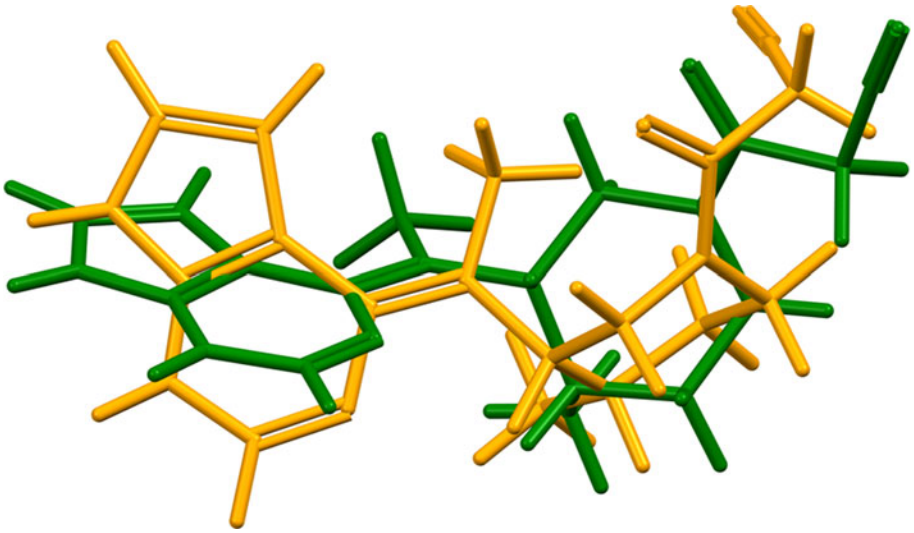

Figure 10. Comparison of the local minimum conformation (green) to the global minimum-energy conformation of an isolated tofacitinib cation (orange). The rms cartesian displacement is 1.794 Å.

TABLE I. Hydrogen bonds (CRYSTAL14) in tofacitinib dihydrogen citrate.

H-Bond	D-H (Å)	H···A (Å)	D···A (Å)	D-H···A (°)	Mulliken Overlap (*e*)	*E* (kcal/mol^{-1})
O56–H64···O59	1.005	1.603	2.599	170.2	0.069	14.4
O55–H63···O21	0.993	1.737	2.711	165.6	0.059	13.3
O60–H61···O58	0.979	1.842*	2.534	125.0	0.054	12.7
N35–H62···O59	1.059	1.606	2.663	175.3	0.086	6.8
N38–H39···O58	1.033	1.763	2.767	162.7	0.066	5.9
C47–H53···N26	1.093	2.529	3.599	165.9	0.014	
C42–H43···O54	1.078	2.430	3.232	130.1	0.012	
C33–H34···O57	1.085	2.235	3.187	145.1	0.025	
C22–H24···O55	1.097	2.594	3.645	160.4	0.015	
C16–H18···N32	1.092	2.672	3.694	155.6	0.010	
C16–H17···O21	1.093	2.678	3.695	154.6	0.011	
C4–H12···N26	1.094	2.532	3.432	138.8	0.012	
C5–H8···O54	1.088	2.284	3.313	156.9	0.025	
C3–H7···O60	1.085	2.106	3.156	162.1	0.034	

*indicates intramolecular.

https://doi.org/10.1017/S0885715621000105 Published online by Cambridge University Press

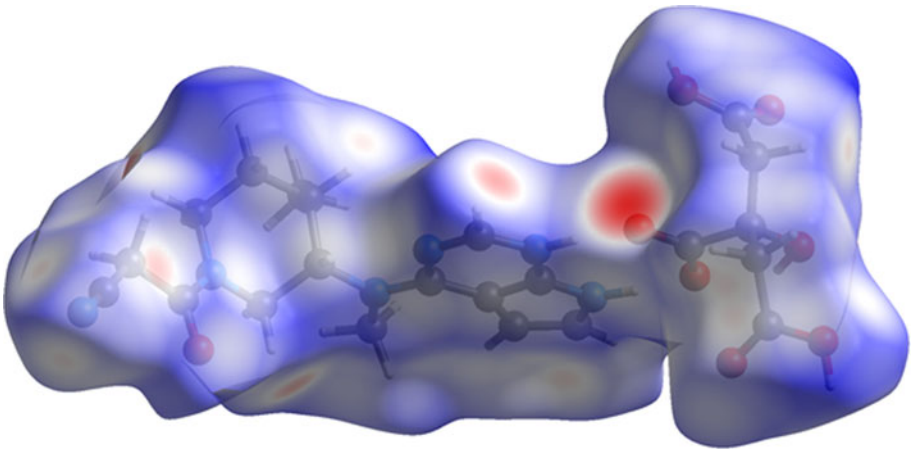

Figure 11. The Hirshfeld surface of tofacitinib dihydrogen citrate. Intermolecular contacts longer than the sums of the van der Waals radii are colored blue, and contacts shorter than the sums of the radii are colored red. Contacts equal to the sums of radii are white.

Wheatley and Kaduk (2019). Several C–H···O and C–H···N hydrogen bonds also contribute to the lattice energy.

The volume enclosed by the Hirshfeld surface (Figure 11; Hirshfeld, 1977; Turner *et al.*, 2017) is 571.98 Å^3, 98.34% of one-fourth the unit cell volume. The molecules are, thus, not tightly packed. All of the significant-close contacts (red in Figure 11) involve the hydrogen bonds. The volume/non-hydrogen atom is 16.1 Å^3.

The Bravais–Friedel–Donnay–Harker (Bravais, 1866; Friedel, 1907; Donnay and Harker, 1937) morphology suggests that we might expect elongated morphology for tofacitinib dihydrogen citrate, with <100> as the principal axes. A second-order spherical harmonic model for preferred orientation was incorporated into the refinement. The texture index was only 1.000(0), indicating that preferred orientation was not present in this rotated capillary specimen. The powder pattern of tofacitinib dihydrogen citrate from this synchrotron data set has been submitted to ICDD for inclusion in the Powder Diffraction File.

IV. DEPOSITED DATA

The Crystallographic Information Framework (CIF) files containing the results of the Rietveld refinement (including the raw data) and the DFT geometry optimization were deposited with the ICDD. The data can be requested at info@icdd.com.

ACKNOWLEDGEMENTS

Use of the Advanced Photon Source at Argonne National Laboratory was supported by the U.S. Department of Energy, Office of Science, Office of Basic Energy Sciences, under Contract No. DE-AC02-06CH11357. This work was partially supported by the International Centre for Diffraction Data. We thank Lynn Ribaud and Saul Lapidus for their assistance in the data collection, and Andrey Rogachev for the use of computing resources at IIT.

CONFLICTS OF INTEREST

The authors have no conflicts of interest to declare.

Altomare, A., Cuocci, C., Giacovazzo, C., Moliterni, A., Rizzi, R., Corriero, N., and Falcicchio, A. (**2013**). "EXPO2013: a kit of tools for phasing crystal structures from powder data," J. Appl. Crystallogr. **46**, 1231–1235.

Bernstein, J., Davis, R. E., Shimoni, L., and Chang, N. L. (**1995**). "Patterns in hydrogen bonding: functionality and graph set analysis in crystals," Angew. Chem. Int. Ed. Engl. **34**, 1555–1573.

Blumenkopf, T. A., Flanagan, M. E., and Munchhof, M. J. (**2001**). "Pyrrolo [2,3-d]pyrimidine compounds," International Patent Application WO 01/42246 A2.

Bravais, A. (**1866**). *Etudes Cristallographiques* (Gauthier Villars, Paris).

Bruno, I. J., Cole, J. C., Kessler, M., Luo, J., Motherwell, W. D. S., Purkis, L. H., Smith, B. R., Taylor, R., Cooper, R. I., Harris, S. E., and Orpen, A. G. (**2004**). "Retrieval of crystallographically-derived molecular geometry information," J. Chem. Inf. Sci. **44**, 2133–2144.

Dassault Systèmes (**2020**). *Materials Studio 2020* (BIOVIA, San Diego, CA).

Donnay, J. D. H. and Harker, D. (**1937**). "A new law of crystal morphology extending the law of bravais," Am. Mineral. **22**, 446–447.

Dovesi, R., Orlando, R., Erba, A., Zicovich-Wilson, C. M., Civalleri, B., Casassa, S., Maschio, L., Ferrabone, M., De La Pierre, M., D-Arco, P., Noël, Y., Causà, M., and Kirtman, B. (**2014**). "CRYSTAL14: a program for the ab initio investigation of crystalline solids," Int. J. Quantum Chem. **114**, 1287–1317.

Etter, M. C. (**1990**). "Encoding and decoding hydrogen-bond patterns of organic compounds," Acc. Chem. Res. **23**, 120–126.

Favre-Nicolin, V. and Černý, R. (**2002**). "FOX, 'free objects for crystallography': a modular approach to ab initio structure determination from powder diffraction," J. Appl. Crystallogr. **35**, 734–743.

Flanagan, M. E. and Li, Z. J. (**2002**). "Novel crystalline compound," European Patent EP 1,451,192 B1.

Friedel, G. (**1907**). "Etudes sur la loi de bravais," Bull. Soc. Fr. Mineral. **30**, 326–455.

Gates-Rector, S., and Blanton, T. (**2019**). "The powder diffraction file: a quality materials characterization database," Powder Diffr. **39**, 352–360.

Gatti, C., Saunders, V. R., and Roetti, C. (**1994**). "Crystal-field effects on the topological properties of the electron-density in molecular crystals - the case of urea," J. Chem. Phys. **101**, 10686–10696.

Groom, C. R., Bruno, I. J., Lightfoot, M. P., and Ward, S. C. (**2016**). "The Cambridge Structural Database," Acta Crystallogr. Sect. B: Struct. Sci., Cryst. Eng. Mater. **72**, 171–179.

Hirshfeld, F. L. (**1977**). "Bonded-atom fragments for describing molecular charge densities," Theor. Chem. Acta **44**, 129–138.

Kaduk, J. A., Crowder, C. E., Zhong, K., Fawcett, T. G., and Suchomel, M. R. (**2014**). "Crystal structure of atomoxetine hydrochloride (Strattera), $C_{17}H_{22}NOCl$," Powder Diffr. **29**(3), 269–273.

Lee, P. L., Shu, D., Ramanathan, M., Preissner, C., Wang, J., Beno, M. A., Von Dreele, R. B., Ribaud, L., Kurtz, C., Antao, S. M., Jiao, X., and Toby, B. H. (**2008**). "A twelve-analyzer detector system for high-resolution powder diffraction," J. Synch. Rad. **15**(5), 427–432.

https://doi.org/10.1017/S0885715621000105 Published online by Cambridge University Press

Lei, X., Peng, J., and Guo, Z. (**2015**). "Tofacitinib citrate," International Patent Application WO 2015/051738 A1.

Macrae, C. F., Sovago, I., Cottrell, S. J., Galek, P. T. A., McCabe, P., Pidcock, E., Platings, M., Shields, G. P., Stevens, J. S., Towler, M., and Wood, P. A. (**2020**). "*Mercury 4.0*; from visualization to design and prediction," J. Appl. Crystallogr. **53**, 226–235.

MDI (**2020**). *JADE Pro version 7.8* (Computer software), Materials Data, Livermore, CA, USA.

O'Boyle, N., Banck, M., James, C. A., Morley, C., Vandermeersch, T., and Hutchison, G. R. (**2011**). "Open babel: an open chemical toolbox," J. Chem. Informatics **3**, 33. doi:10.1186/1758-2946-3-33.

Rammohan, A. and Kaduk, J. A. (**2018**). "Crystal structures of alkali metal (group 1) citrate salts," Acta Crystallogr. Sect. B: Struct. Sci., Cryst. Eng. Mater. **74**, 239–252. doi:10.1107/S2052520618002330

Shields, G. P., Raithby, P. R., Allen, F. H., and Motherwell, W. S. (**2000**). "The assignment and validation of metal oxidation states in the Cambridge Structural Database," Acta Crystallogr. Sect. B: Struct. Sci., Cryst. Eng. Mater. **56**(3), 455–465.

Silk Scientific (**2013**). *UN-SCAN-IT 7.0* (Silk Scientific Corporation, Orem, UT).

Sykes, R. A., McCabe, P., Allen, F. H., Battle, G. M., Bruno, I. J., and Wood, P. A. (**2011**). "New software for statistical analysis of Cambridge Structural Database data," J. Appl. Crystallogr. **44**, 882–886.

Toby, B. H. and Von Dreele, R. B. (**2013**). "GSAS II: the genesis of a modern open source all purpose crystallography software package," J. Appl. Crystallogr. **46**, 544–549.

Turner, M. J., McKinnon, J. J., Wolff, S. K., Grimwood, D. J., Spackman, P. R., Jayatilaka, D., and Spackman, M. A. (**2017**). *CrystalExplorer17* (University of Western Australia). Available at: http://hirshfeldsurface.net.

van de Streek, J. and Neumann, M. A. (**2014**). "Validation of molecular crystal structures from powder diffraction data with dispersion-corrected density functional theory (DFT-D)," Acta Crystallogr. Sect. B: Struct. Sci., Cryst. Eng. Mater. **70**(6), 1020–1032.

Wang, J., Toby, B. H., Lee, P. L., Ribaud, L., Antao, S. M., Kurtz, C., Ramanathan, M., Von Dreele, R. B., and Beno, M. A. (**2008**). "A dedicated powder diffraction beamline at the advanced photon source: commissioning and early operational results," Rev. Sci. Instrum. **79**, 085105.

Wavefunction, Inc. (**2020**). Spartan '18 Version 1.4.5, Wavefunction Inc., 18401 Von Karman Ave., Suite 370, Irvine, CA 92612.

Wheatley, A. M. and Kaduk, J. A. (**2019**). "Crystal structures of ammonium citrates," Powder Diffr. **34**, 35–43.

Wilcox, G. E., Koecher, C., Vries, T., Flanagan, M. E., and Munchhof, M. J. (**2002**). "Optical resolution of (1-benzyl-4-methylpiperidin-3-yl)-methylamine and the use thereof for the preparation of pyrrolo-2,3-pyrimidine derivatives as protein kinases inhibitors," International Patent Application WO 02/096909 A1.

https://doi.org/10.1017/S0885715621000105 Published online by Cambridge University Press